VIII International Conference on Fracture Mechanics of Concrete and Concrete Structures
FraMCoS-8
J.G.M. Van Mier, G. Ruiz, C. Andrade, R.C. Yu and X.X. Zhang (Eds)

MECHANICAL BEHAVIOUR OF REINFORCED STONE BEAMS IN BENDING: EXPERIMENTAL AND NUMERICAL RESULTS

O. OMIKRINE-METALSSI[1*], C. DOUTHE[1], M. PRESEPI[2] AND M. BROCATO[2]

[1] Université Paris-Est
IFSTTAR, SOA, 58, Bvd Lefebvre, F-75732, Paris, France
e-mail: othman.omikrine-metalssi@ifsttar.fr, www.ifsttar.fr

[2] Université Paris-Est, Ecole Nationale Supérieure d'Architecture Paris-Malaquais
14, rue Bonaparte, 75272-Paris-France
e-mail: info@paris-malaquais.archi.fr, www.paris-malaquais.archi.fr

Key words: Masonry structures, Dimension stone, Reinforcement, Bending, Digital image correlation, Numerical modeling.

Abstract: Masonry structures such as bridges, civil and worship buildings or monuments represent the largest part of the construction heritage in the world. They are indeed remarkably durable and earthquake resistant if they were correctly designed. Beside they also have very interesting environmental properties, notably in terms of life cycle analysis, so that stone and masonry have a good potential as building materials for modern architecture. The understanding of their mechanical behaviour is hence necessary to develop proper design methods for the prediction of displacements, crack opening or plastic failure in the sense of Eurocode or other modern design recommendations.
The proposed article is dedicated to the study of an innovative system of reinforced stone beam. It consisted in performing experimental tests on three specimens tested in the laboratory where two measurement methods have been applied (extensometers and image correlation). Moreover, numerical calculations have been conducted with three dimensional nonlinear finite elements program to predict displacement discontinuities in the studied structures.

1 INTRODUCTION

Symbolic pieces of art such as bridges, civil and worship buildings or monuments have been made of stone throughout human history [1]. These structures represent the largest part of the construction heritage in the world. They are remarkably durable with the ability to endure and maintain their characteristics of strength, widespread and earthquake resistant and they resist fire, water, and insect damage and have very interesting environmental properties, especially in terms of life cycle analysis notably if the stone is produced locally [2-5]. There seems hence to be no reason why stone doesn't have a good potential as building materials for modern architecture [6].

From a mechanical point of view, the main characteristics of stones are a high compressive strength and an almost null tensile strength. Therefore, in historical structures, the use of stone is mostly restricted to compression members (piers, arches, walls and vaults). Many masonry structures are however hyperstatic, so that, if some bending is induced, it can be resisted by a loss of hyperstaticity through a change of geometry and the opening of joints in a similar way to plastic hinges in metal structures [7]. In the best cases, this way of resisting bending moments leads to anaesthetic consequences and cracking but sometimes also leads to

collapse. To introduce more ductility, recent researches investigated innovative systems by playing with the geometry of joints [8-9] or the arrangement of stones [10], but the most current solution which is often used in restoration of historical buildings is the reinforcement of the stones by composite materials and/or steel bars [11-13] especially in seismic area [14-15].

Such solutions of reinforcement have also been developed for newly built structures for a century or more: for example a system of arch for coupling the properties of steel and stone [9]. However, it is necessary to have a good understanding of their mechanical behaviour to develop proper design methods for the prediction of displacements, crack openings or plastic failure in the sense of Eurocode or other modern design standards.

The aim of this work is the study of an innovative system of reinforced stone beam which will be further used for the calibration of numerical models and the development of design recommendations. Indeed, tests on three beams under four points bending have been performed in the laboratory. Typical load-displacement curves have been produced from data recorded by three load cells and a dozen of extensometers or strain gages measuring characteristic displacements, end-rotations and crack opening. These measures have been completed with "Digital Image Correlation-DIC" which allows for the quantification of relative displacements of the blocks when loaded. The beams have been subjected to oligo-cyclic loading to evidence hysteresis effects.

Numerical calculations have been conducted with the three dimensional nonlinear finite elements program called CESAR-LCPC. Spatial representation of the beam has been investigated and modeled. The objective of the modeling is to predict displacement discontinuities in the structures taking into account the friction and shear between the stones and also the cracks opening that result from the applied loading.

2 EXPERIMENTAL STUDY

2.1 Description of the beams

Three reinforced dimension stone beams with the dimensions of 20.0 cm width, 25.0 cm height, 18.75 cm length and an inclination of the contact surfaces of 10° are manufactured according to the sketch of Figure 1. These beams are made of 15 stone blocks which physical properties are given in Table 1. They have been assembled using hydraulic lime mortar joints and reinforced with a steel bar (HA12) glued with epoxy to the underside of each beam in a deep groove of a half diameter (Figure 2). The average length of the beams is 289.2 cm with joints approximately 5 mm thick.

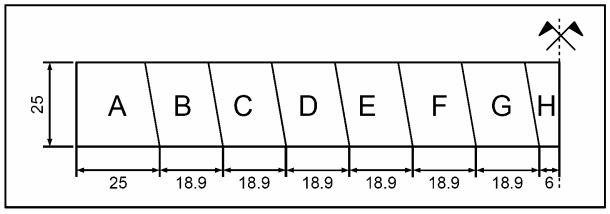

Figure 1. Scheme of the reinforced freestone beams

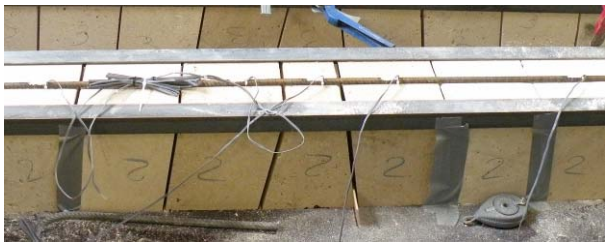

Figure 2: Assembling of the beam and reinforcement

Table1: Physical properties of the stone

Apparent density (kg/m^3)	Porosity (%)	Sound velocity (m/s)	Tensile Strength (MPa)
1660	38.8 ± 1.1	2560 ± 80	1.6 ± 0.1
Compressive strength (MPa)		Young modulus (GPa)	Poisson ratio
10.2 ± 1.5		7.3	0.23

2.2 Testing procedure

A four-points bending test is performed on each beam until rupture by using the experimental setup shown in Figure 3. The beams are placed on rollers located in the middle of each end-block where the translation of one of them is fixed so that the beam is isostatic.

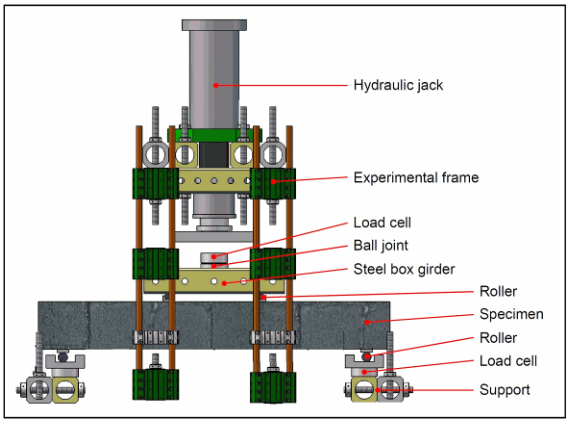

Figure 3: Test setup

The load is applied with a hydraulic jack with a capacity of 1000 kN and distributed with a stiff metallic box girder (weighting approximately 360 kg). The distance between two loading cylinders is about 750 mm (see Figure 4). Recording of data is started before the girder is set, so that the load induced by the girder is taken into account. Then an oligo-cyclic loading program is applied. It consists on three sets of three cycles with amplitude of 3 kN each (from 1 to 4 kN, 4 to 7 kN and 7 to 10 kN). The tests are ended with a progressive increase of the load until failure with a speed of 1 mm in 2 minutes.

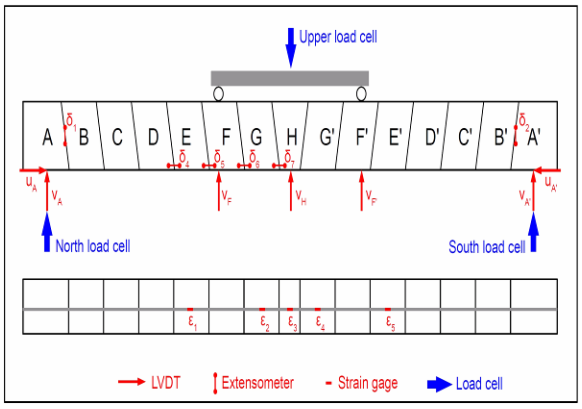

Figure 4: Details of measuring devices

The deflections of the specimens at mid-spans and at the level of the applied loads are measured using linear variable differential transducers (LVDTs). Four other LVDTs are also set to measure the displacement of the support horizontally and vertically. Furthermore five strain gauges are mounted symmetrically on the reinforcing bars to measure their deformations. At the level of four joints between blocks (D-E, E-F, F-G, G-H), extensometers are also installed horizontally on the side of the beam (30 mm above the edge) to measure the joint opening evolution. Two others extensometers are installed vertically to measure the slip between the blocks at the supports. Three load cells complete the measuring devices (see Figure 4). Computer aided data acquisition systems are used to record continuously, load, deflection, slip and strain at a frequency of 2 Hz.

Moreover, "Digital Image Correlation-DIC" technique [16-17] is applied to measure two dimensional deformations in the central part of the beams, covering from block E to block E' (see Figure 4). Taking every 0.5 kN images (similar to that of Figure 5), a monitoring of the deformations can be obtained from a standard digital camera (Nikon DS 300). The specimen are cleaned to achieve a smooth surface and then covered with black and white random colour pattern (Figure 5).

Figure 5: Image analysis disposal with feedback of the load in the foreground

2.3 Experimental results

2.3.1 Global behavior

To illustrate the global behaviour of the beams, three load–deflection curves are plot. The first one, that of Figure 6, shows the total load (the sum of the North and South reaction)

in function of the deflection at the mid-span for the three beams (given by the v_H LVDT in Figure 4).

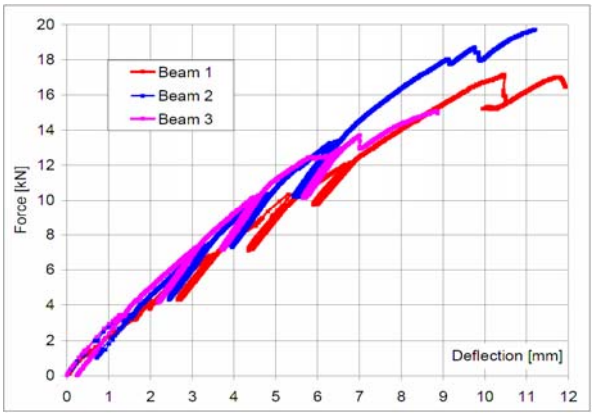

Figure 6: Global behavior of the three specimens

Globally the beams behave in a very similar way and two different linear behaviours are clearly visible within each load-deflection curve: one when the beam reaches for the first time a given level of load, the other (the highest) when the beam is submitted to a cyclic load. The average value for the three beams are 2.1 ± 0.2 kN/mm for the initial stiffness and 3.1 ± 0.3 kN/mm for the cyclic stiffness. The difference between both stiffness is significant (about 30 % less for the first loading) and can be due to the irreversible crushing of the joints which causes displacements that are never recovered.

Despite a good reproducibility, a small decrease of the two stiffness is observed when the load increases; this is probably due to the beginning of the beam damaging at joints. For the three beams collapse starts with a cracking of one or more blocks in the lateral part of the beam where shear forces are constant (between blocks C and F). The crack appears in the upper part of the block and goes parallel to the direction of the principal compression which means here approximately perpendicular to the joints (see Figure 7).

The maximum load reached by the beam depends directly on the quality of the mortar of the joints which have been made here by non expert workers (see Figure 8). The three beams hence reached 17.1 kN, 19.7 kN and 15.1 kN respectively.

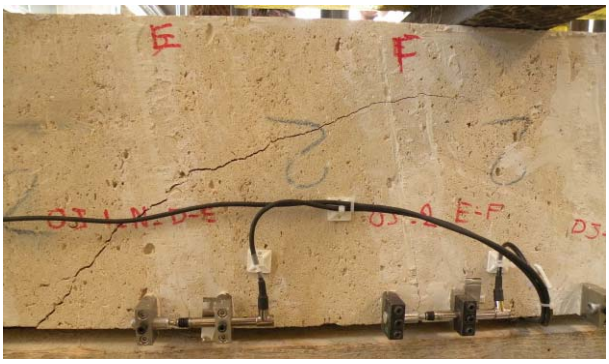

Figure 7: Through-crack from block D to F in beam 2

Figure 8: Irregularity of the mortar for the stone assemblage

Moreover the behaviour of the beam remains symmetrical during the whole test as it can be seen in Figure 9 which represents the vertical deflection of three blocks located in the central part of beam 1 (block F and F' at the level of the applied loads and block H at the mid-span). As expected from standard beam theory, the displacements of block F and F' are almost equal and slightly lower than that of block H (here about 7%).

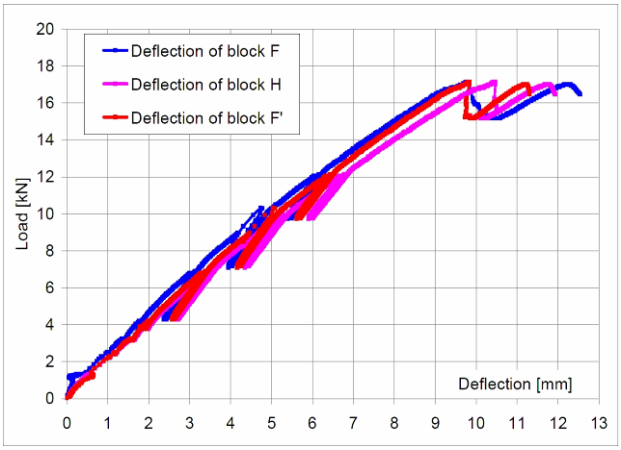

Figure 9: Deflections of blocks F, H and F' in beam 2

Finally, all these results are confirmed by digital image correlation (DIC). Indeed, when comparing two measures of the deflections, one by LVDT and the other by DIC, a very good correlation is observed with differences lower than 5 %. Figure 10 which shows for example the comparison of the deflection at mid-span illustrates this fact very well. These results prove the accuracy of quantitative analyses based on the DIC technique so that it will be used in the following for the study of the joints opening.

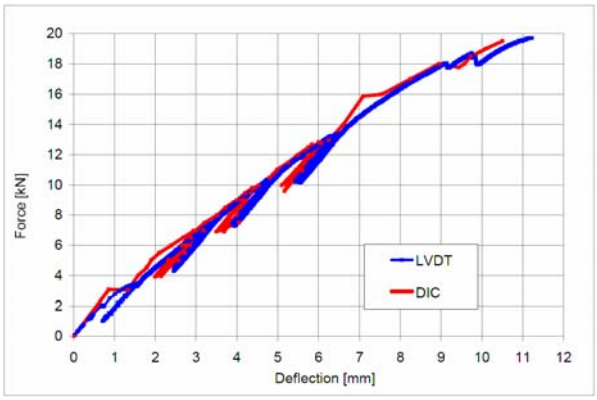

Figure 10: Comparison of deflections at mid-span obtained by LVDT and DIC

2.3.2 *Joints opening measurements*

Figure 11 shows the results of the joints opening measurements which concern the three beams at the level of two joints (D-E and G-H). The joints opening at mid-span (G-H) is the most important as expected from the bending moment diagram in the beam. Moreover, one notes that the three beams do not behave in the same manner and that the gap between the opening of joints D-E and G-H is much higher in beam 2 than in beam 1. The scattering of results between specimens is thus more important for joints opening than for the deflections (see Figure 6). Obviously this is to be related to the fact that joints' opening is a local information which is much more influenced by local default (mainly the heterogeneity of the hydraulic lime mortar) than the deflection which is a global information that aggregates and averages these defaults.

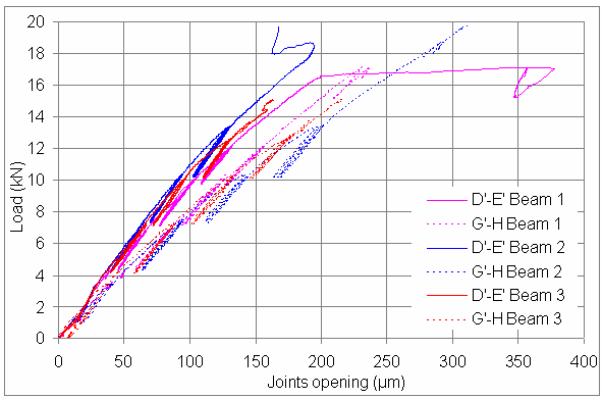

Figure 11: Joints opening in joints D-E and G-H for the three beams

To confirm these results, a comparison between the joints opening measurements using extensometers and images analysis is carried out. Figure 12 shows a comparison of both techniques for two joints (F-G and G-H) of beam 2. Although the values by the DIC technique are quite dispersed, they are in good correlation with the extensometers measurements. This dispersion can be explained by the fact that the order of magnitude of the displacements measured here is too close to that of the precision of the method (which is linked with the characteristic size of the color pattern on the beam ≈ 1 mm and that of a pixel ≈ 200 µm). Hence, on a single measurement, DIC allows merely having qualitative results concerning joints opening and it must be coupled to an other experimental technique as in this study.

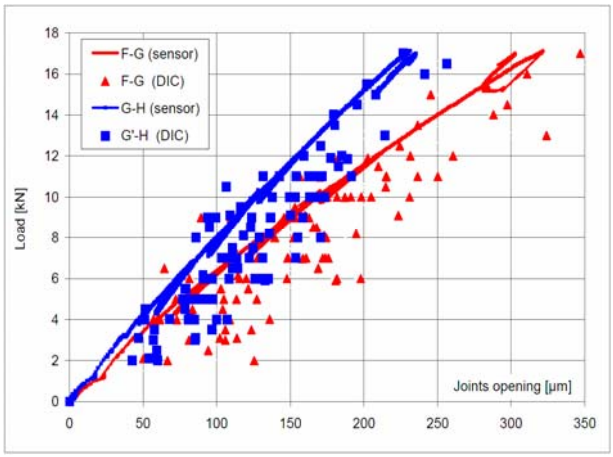

Figure 12: Comparison of joints opening obtained by extensometer and DIC

2.3.3 Sliding between blocks at supports

The phenomenon investigated here is the transmission of shear forces to the support. In the proximity of the end blocks (A and A'), the direction of the principal compression is inclined respectively to the normal of the joint, so that there is a chance that sliding is activated when the load increases. To monitor this sliding, two extensometers have been set vertically between the blocks A-B and A'-B'. The registered data for the three beams is reported in Figure 13. Up to 6 kN, all the curves are very similar. For higher load, the beams who have the lower quality of end joints (beam 1 in A'-B' and beam 2 in A-B) start sliding significantly on one side, on the contrary to beam 3 where the two curves (A-B and A'-B') remain superimposed until break. It is however remarked that once it starts sliding, the behaviour is very similar to what had been observed for the deflection or the joint opening: there is one stiffness of the joint for the first loading and one stiffness for repeated loading. And in the case of sliding, the difference between the two stiffness is considerable (about 50 times lower when sliding is activated). This shows once again that special attention should be paid to the realization of the lime mortar.

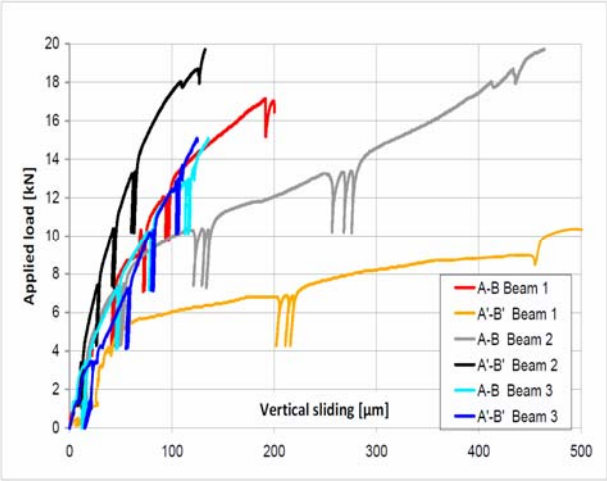

Figure 13: Sliding of joints between end-blocks

3 MODELLING

3.1 Finite Element model

The Finite Element software chosen to simulate the four-point bending tests on beam is CESAR-LCPC developed by the French Institute of Science and Technology for Transport and Civil Engineering (IFSTTAR, formerly LCPC) [18]. In this modeling, the module MCNL (Calculation of non-linear structures) is associated with the Mohr-Coulomb criterion that involves both the maximum shear and average stress. This criterion is underpinned by the concept of friction, and assumes that the maximum shear that can undergo the material is much larger when the normal stress of compression is high (see Eq. 1).

$$|\tau| \leq C + \sigma.\tan(\varphi) \qquad \text{(Eq. 1)}$$

where σ is the normal stress, τ is the shear stress, φ is the friction angle and C is the cohesion.

3.2 Materials, mesh characteristics and parameters

The stone behaviour is supposed to be linear elastic, while the joint mortar behaviour is assumed to be elaso-plastic. Due to the symmetry of the problem, only a quarter of the beam is modelled and discretized with quadratic solid elements (20 nodes per element). A total of 1920 three dimensional elements and 11136 nodes in the entire model has been used for the finite element calculations. The numerical simulations have been carried out assuming Young's modulus and Poisson's ratio equal to E_s = 8.4 GPa and υ_s = 0.25 for stone blocks and E_m = 60 MPa and υ_m = 0.30 for mortar, respectively. For the steel bar, the section is equal to S = 0.565 cm^2 (1/2 HA12) and the Young modulus equal to E_{st} = 210 GPa. For the Mohr-Coulomb criterion parameters, the cohesion and the friction angle have been taken as C = 0.1 MPa and φ = 25°, respectively.

Concerning the boundary conditions, the perpendicular displacements are restrained perpendicularly to the plane of symmetry (pink coloured element on Figure 14). At supports, vertical displacements are equal to zero. Finally, the beam is subjected to its own weight and to oligocyclic loading as it is presented in the experimental part of this study.

During testing, the load is applied by the hydraulic jack on the blocks F and F' of the beam with a surface of 8 x 20 cm. To model this load, the maximum stress (σ_{max} = 0.615 MPa) is calculated by taking into account the maximum load reached before failure (F_{max} = 19.7 kN). Thus, this stress value has been applied in 74 increments which describe the experimental oligocyclic loading.

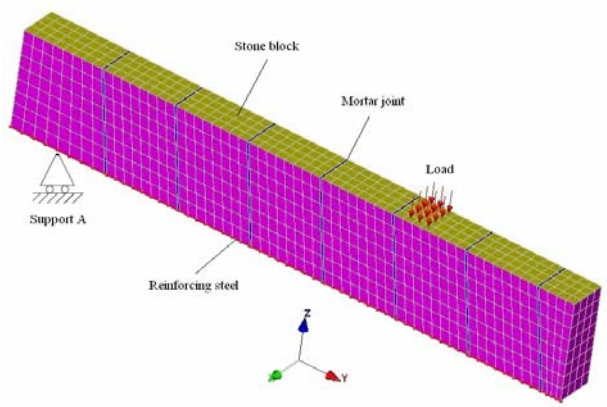

Figure 14: Geometrical characteristics and finite element mesh for the studied beam

3.3 Results

Figure 15 presents the iso-values of vertical displacements in the studied beam. It shows an important sliding between blocks A and B with a vertical displacement of the beam end. In addition, there is a crush in the upper part of the beam (compressed part) and a stretching of these joints in the lower part (tension part). Finally, one notes also a rotation of the beam around the support that is presented by the displacement vectors in Figure 15. This rotation increases when one approaches the support.

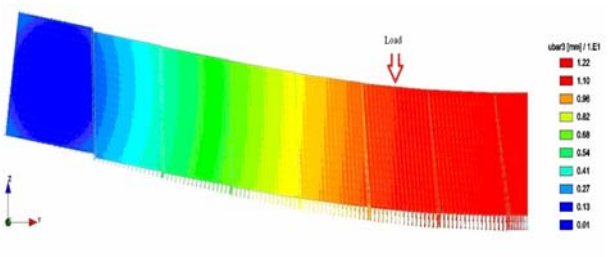

Figure 15: Iso-values of vertical displacements in the studied beam just before failure

On the other hand, Figure 16 shows the iso-values of tensile stress in the studied beam. As is clearly shown, these tensile stresses are concentrated at the level of the steel bar, especially near the joints. They become higher when one approaches the center of the beam with a maximum value of 34.5 MPa in the stone. Of course this value is not realistic because the tension in the stone cannot exceed 1.5 Mpa. A more realistic model would take into account the fact that the steel bar is not a line but a cylinder and the resin is elastic and distribute the stress concentration. Due to the perfect connection between the volume elements representing the stone and linear elements representing the steel bar, the stress in the steel is equal to 865 MPa. Again this is a numerical artifact which could be avoided with a finer model locally.

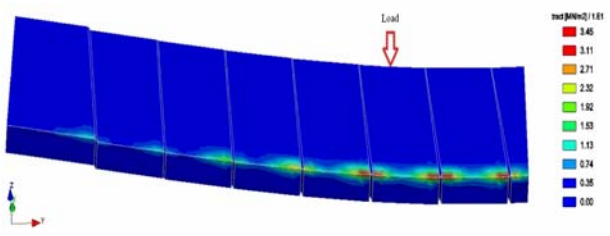

Figure 16: Iso-values of tensile stress in the studied beam just before failure

Besides, Figure 17 shows the evolution of the deflection vs. the applied load at the level of blocks H (mid-span) and F (zone of applied load). Despite a slight curvature, the deflections D_H and D_F have almost a linear behavior with $D_H > D_F$ for the same load value as one would expect from the bending moment diagram. Moreover, the slopes of D_H and D_F are higher in cycles than in the rest of the

curves. These modeling curves have quite the same evolution and values as the experimental ones given in Figure 9.

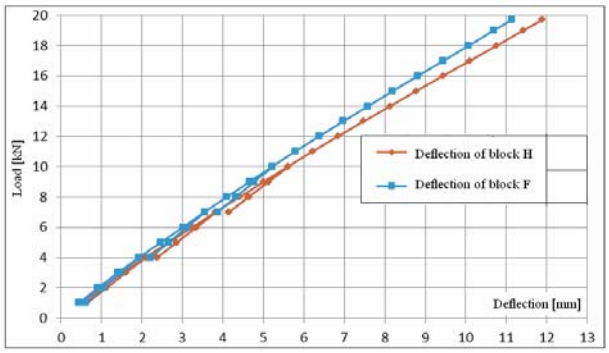

Figure 17: Evolution of deflections at blocks H and F vs. applied loads

Concerning the joints opening, Figure 18 presents their evolution for different loads. As is clearly shown, the non-linearity of the curves is especially highlighted in the early loading (between 0 and 5 kN). After this load, the behavior of the joints seems to be perfectly bi-linear with an increase of the slopes in cycles. One notes also a strong similarity between the evolution of the joints H-G and F-E whose curves are almost confounded. Here also, these curves have quite the same evolution and values as the experimental ones given in Figure 11.

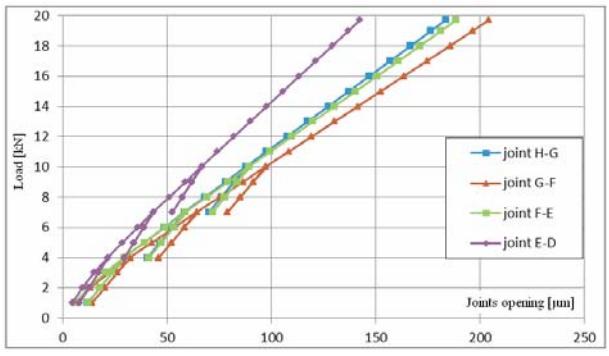

Figure 18: Evolution of joints opening vs. applied loads

Finally, Figure 19 presents the evolution of the sliding between blocks A and B vs. the applied load. This sliding progresses weakly and almost linearly with a strong slope up to 9 kN. Once this load is reached, the sliding becomes much more important with a week slope. A load close to 9 kN appears to be a threshold for activation of sliding at the joint A-B. As for the case of deflection and joints opening results, the experimental and numerical sliding between blocks A and B have quite the same evolution (see Figure 13).

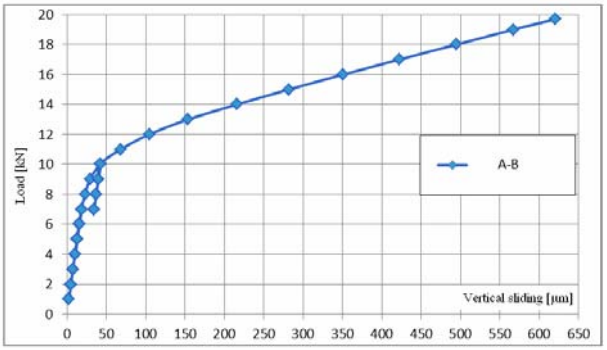

Figure 19: Evolution of vertical sliding between blocks A and B vs. applied loads

4 CONCLUSION

Three prototypes of reinforced dimension stone beams have been tested. Their global and local mechanical behaviours have been investigated and the results of these investigations have shown that the idea of developing reinforced stone beams in a similar way to reinforced concrete beam had a good potential. Indeed the prototypes showed a clear beam behaviour where external forces are resisted by bending and not solely by compression like in usual masonry structures. Bending moments are transmitted in compression by the stone and in tension by the reinforcement; shear forces in compression trough the joints and in tension by the stone. A strut-and-tie model should thus be transposable to this kind of structure.

For the three prototypes, the bonding between the stone and the steel bar was not damage and failure occurred in the stone due to tension forces in the shear area. The limiting issue here is the tensile strength of the stone and not its shear strength. One should thus think of an adequate way of reinforcing the beam to resist shear. Apart from that, the general behaviour of the beam could benefit from an improvement of the manufacturing process and from an “industrialisation” of the joints technique which would increase the

uniformity of their characteristics. Development should also be made to protect the reinforcement for external aggression.

Furthermore, various measuring techniques (LVDT, gages, DIC) have been used in this work and they have shown good correlation. However, local results given by DIC have shown some discrepancy, so that in the future more attention should be paid to the definition of the investigated area and to the size of uncertainties that goes with it.

Finally, numerical results are quite satisfactory in terms of quality, although quantitatively there remains a significant gap between numerical and experimental results for some variables (eg openings joints). It seems however that this numerical model allows reproducing the physical behavior of the stone beam.

ACKNOWLEDGEMENTS

The authors whish to acknowledge SNBR (www.snbr-stone.com*)* who offered the stone and supports this research on modern stone architecture from the beginning. They also would like to thanks F. Martineau for carrying out the tests on the stone and A. Degrange for its help in the data processing.

REFERENCES

[1] Nicholas T., Behavioural inferences from early stone artefact assemblages: an experimental model, *Journal of Human Evolution*, *Volume 16, Issues 7–8*, *November–December 1987*, *Pages 763-787.*

[2] Murray-Wooley C and Richard T., The dry Stone Age: the Dry Stone Conservancy Promotes an Ancient Craft**.** Cultural Resource Management, 1997, Vol 20, no 12, pp 17-19.

[3] Anon., 1983. The selection of natural building stone. Digest. 260. Watford: Building Research Establishment. Her Majesty's Stationary Office.

[4] Bruegmann, R., Architecture Confronts Environmental Technology: A Historical Perspective. In D. Watson, (ed.), *Energy Conservation Through Building Design,* McGraw-Hill Book Co, 1979.

[5] Morela J.C., Mesbaha A., Oggerob M. and Walkerc P., Building houses with local materials: means to drastically reduce the environmental impact of construction, Building and Environment 36 (2001) 1119–1126.

[6] Benavente D., García del Cura M.A., Fort R. and Ordóñez S., Durability estimation of porous building stones from pore structure and strength, Engineering Geology 74 (2004) 113– 127.

[7] Heyman J. The Stone Skeleton: Structural Engineering of Masonry Architecture, Cambridge University Press, (1997), pp. 172.

[8] Bagnéris M., Dubois F., Martin A., Mozul R., Taforel P., De l'intérêt de la courbure dans les interfaces : application aux structures en pierre, CSMA 2011 10e Colloque National en Calcul des Structures,Mai 2011, Giens (in French)

[9] Fallacara G, Brocato M, Tamborero L, E. E. Viollet-le-Duc et les ossatures constructives mixtes: spéculations morphologiques et constructives sur le thème de l'arc armé, IIe colloque international de Pierrefonds, septembre 2010 (in French).

[10] Brocato M., Mondardini L., A new type of stone dome based on Abeille's bond, International Journal of Solids and Structures 49 (2012) 1786–1801

[11] Venkatarama Reddy, B. and Gupta, A. (2006). "Tensile Bond Strength of Soil-Cement Block Masonry Couplets Using Cement-Soil Mortars." *J. Mater. Civ. Eng.*, 18(1), 36–45.

[12] Elmalich D. and Rabinovitch O., Masonry and monolithic circular arches strengthened with composite materials – A finite element model, Computers and Structures 87 (2009) 521–533.

[13] De Felice G, Assessment of the load-carrying capacity of multi-span masonry arch bridges using fibre beam elements, Engineering Structures 31 (2009) 1634-1647.

[14] Tao Y., Stratford T.J. and Chen J.F., Behaviour of a masonry arch bridge repaired using fibre-reinforced polymer composites, Engineering Structures 33 (2011) 1594–1606.

[15] Feilden B, Between Two Earthquakes: Cultural Property in Seismic Zones, Getty Conservation Institute; 1 edition (October 1, 1987).

[16] Kozicki J and Tejchman J, Experimental Investigations of Strain Localization in Concrete using Digital Image Correlation (DIC) Technique, *Archives of Hydro-Engineering and Environmental Mechanics,* Vol. 54 (2007), No. 1, pp. 3–24.

[17] Chu T C, Ranson W F, Sutton M A and Peters W H, Application of digital-image-correlation techniques to experimental mechanics. *Experimental Mech.* 25 (1985): 232–244.

[18] Humbert, P., Dubouchet, A., Fezans, G. & Remaud, D., 2005. CESAR-LCPC, un progiciel de calcul dédié au génie civil, *Bull. des laboratoires des ponts et chaussées*, 256-257, 7-37, LCPC, Paris.